Growth of Vertically Aligned Nitrogen-Doped Carbon Nanotubes: Control of the Nitrogen Content over the Temperature Range 900−1100 °C

Yun Tack Lee, Nam Seo Kim, Seung Yong Bae, and Jeunghee Park*

Department of Chemistry, Korea University, Jochiwon 339-700, South Korea

Soo-Chang Yu

Department of Chemistry, Kunsan National University, Chonbuk 573-701, South Korea

Hyun Ryu and Hwack Joo Lee

Korea Research Institute of Standards and Science, Daejeon 305-600, South Korea

Received: November 13, 2002; In Final Form: June 9, 2003

Nitrogen-doped carbon nanotubes were grown vertically aligned on the iron nanoparticles deposited on silicon substrates, by thermal chemical vapor deposition of methane/ammonia and acetylene/ammonia mixtures in the temperature range 900−1100 °C. The concentration of the nitrogen atoms has been controlled in the range 2−6 atomic %, by the flow rate of ammonia. All nanotubes exhibit a bamboo-like structure over this temperature range. The growth rate is insensitive to this nitrogen content, but the structure is strongly dependent on it. As the nitrogen content increases, the thicker compartment layers form uniformly at a regular distance and the relative amount of crystalline graphitic sheets is notably reduced. Electron energy-loss spectroscopy reveals the higher nitrogen concentration and the lower crystallinity for the compartment layers compared to the wall. The growth of nitrogen-doped carbon nanotubes has been explained using a base growth mechanism proposed for carbon nanotubes. We suggest that the nitrogen doping would produce more flexible compartment layers connecting the wall under a less strain.

1. Introduction

Carbon nanotubes (CNTs) are an important focus of current research because of many potential applications including field emission displays and radiation source,[1−3] conductive and high-strength composites,[4,5] nanoscale semiconductor devices,[6−8] energy storage devices,[9] and hydrogen storage media.[10] The CNTs are usually made by arc discharge, laser vaporization, pyrolysis, or chemical vapor deposition (CVD).[11−16]

Synthesis of nitrogen (N)-doped CNTs has recently been considered as a possible method to control the electronic properties of CNTs in a well-defined way. An enhancement of conductivity is expected, because the additional electrons contributed by the nitrogen atom provide electron carriers for the conduction band.[17] The advantage of such nanotubes is that their electronic properties are primarily determined by the composition and are thus relatively easy to control. Many research groups reported the synthesis of the N-doped CNTs.[17−32] Terrones et al. reported the generation of aligned N-doped carbon nanofibers and CNTs by pyrolyzing various C/N sources, i.e., triazine, melamine, ferrocene/melamine mixture, and ferrocene/C_{60} mixtures, in ammonia atmosphere.[14,17−20] Wang and co-workers adopted a microwave plasma-assisted CVD of methane/nitrogen mixture.[21−24] The Rao group employed the pyrolysis of pyridine over Fe or Co catalyst.[25,26] The pyrolysis of nickel phthalocyanine was used by Yudasaka et al. and Suenaga et al.[27,28] Sung et al. synthesized the N-doped CNTs on a porous alumina template in a microwave-excited plasma of acetylene/nitrogen using an electron cyclotron resonance CVD system. Hot filament CVD of methane/nitrogen/ammonia and pyrolysis of acetylene/ammonia/iron pentacarbonyl mixtures were also used.[29−31] Recently, Zhang and co-workers reported the vertically aligned N-doped CNTs using the pyrolysis of iron phthalocyanine under the ammonia atmosphere.[32] Those works showed that the N-doped CNTs have a bamboo-like structure with distinctive compartment layers. However, the dependence of the growth properties on the N concentration has not been thoroughly examined yet.

In this study, we report a systematic approach to the influence of the N doping on the growth rate and structure of CNTs over the temperature range 900−1100 °C. It would lead eventually to an understanding of the growth mechanism of N-doped CNTs, which is prerequisite for various potential applications. The vertically aligned N-doped CNTs on the iron (Fe) nanoparticles-deposited silicon (Si) substrates were synthesized by thermal CVD of methane (CH_4)/ammonia (NH_3) and acetylene (C_2H_2)/NH_3 mixtures at 900−1100 °C. The Fe catalytic nanoparticles were formed using a simple method: a thin film of ethanol solution containing Fe salt is deposited on the Si substrate, followed by the NH_3 pretreatment at the growth temperature. Configuration and structural characteristics of CNTs have been investigated using electron microscopy and Raman spectroscopy. The composition of nanotubes was determined using X-ray photoelectron spectroscopy (XPS), Auger spectroscopy, and electron energy-loss spectroscopy (EELS).

2. Experimental Section

Some 10 mm × 15 mm size n-type Si(100) substrates were coated with a drop of 0.01 M $FeCl_2 \cdot 4H_2O$ (Aldrich, 99.995%)

* Corresponding author. E-mail: parkjh@korea.ac.kr.

10.1021/jp0274536 CCC: $25.00
Published on Web 11/05/2003

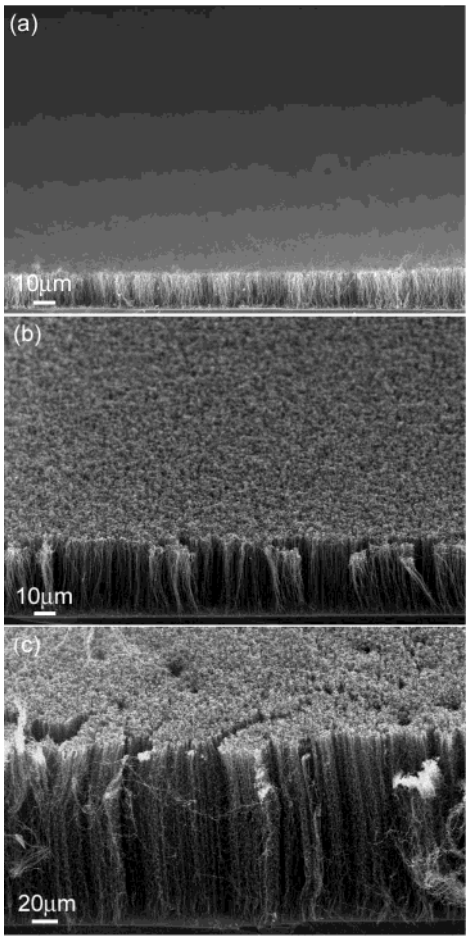

Figure 1. SEM micrographs of the vertically well-aligned N-doped CNTs grown on the Si substrates. The concentration of the N atoms is about 4.5%. (a) The 15 μm long CNTs grown for 10 min at 900 °C, (b) 35 μm long CNTs grown for 10 min at 1000 °C, and (c) 160 μm long CNTs grown for 5 min at 1100 °C.

ethanol solution and then dried. The thickness of the film was adjusted to be ~300 nm. The coated substrates were loaded on a quartz boat placed inside a 2.5 cm diameter and 80 cm long quartz tube reactor. Ar (99.999%) flowed into the reactor in order to prevent the oxidation of Fe while the temperature rises. The substrates were pretreated by NH_3 (99.999%) with a flow rate of 20 sccm for 1−10 min, forming the nanometer-size Fe particles. The CNTs were grown using the mixture of CH_4/NH_3 or C_2H_2/NH_3 for 5−10 min at temperatures ranging between 900 and 1100 °C. The flow rate of CH_4 and NH_3 was 50−300 and 0−150 sccm, respectively. The flow rate of C_2H_2 and NH_3 was 10 and 0−80 sccm, respectively. The reactor was cooled to room temperature under Ar ambient after the growth. Scanning electron microscopy (SEM, Hitachi S-4300), transmission electron microscopy (TEM, Hitachi H9000-NAR, 300 kV), XPS (Physical electronics PHI 5800), Auger spectroscopy (PHI 680), EELS (GATAN GIF-2000) attached to a TEM (Philips CM200, 200 kV), and Raman spectroscopy (Renishaw micro-Raman 2000) using the excitation wavelength as the 514.5 nm line of argon ion laser were employed.

3. Results

(1) Morphology and Growth Rate of the Nanotubes. Figure 1 shows SEM images for the vertically well-aligned nanotubes homogeneously grown on a large area of the substrates. The CNTs grown for 10 min at 900 °C exhibit a length of 15 μm (Figure 1a). The flow rate of CH_4 and NH_3 is 180 and 20 sccm, respectively. The 35 μm long CNTs are grown for 10 min at 1000 °C (Figure 1b). The flow rate of CH_4 and NH_3 is 160 and 40 sccm, respectively. The length of the CNTs grown during 5 min at 1100 °C is 160 μm (Figure 1c). The flow rate of CH_4 and NH_3 is 150 and 50 sccm, respectively. From several experimental runs, the average length of the CNTs grown at 900, 1000, and 1100 °C has been measured as 10 ± 10, 30 ± 20, and 150 ± 25 μm, respectively. Dividing the length by the growth time yields the average growth rate of CNTs, which is 1 ± 1, 3 ± 2, and 30 ± 5 μm/min, respectively, for 900, 1000, and 1100 °C. The growth rate at 900 and 1000 °C is constant during the first 10 min and then decreases as the carbonaceous particles cover the surface of substrate. At 1100 °C the growth rate decreases after 5 min. The number density of CNTs on the substrate is $\sim 10^{10}/cm^2$. The pretreatment condition has been adjusted to form the size and density of nanoparticles suitable to grow the high-density CNTs.

XPS and Auger analyses show that these CNTs are doped with the same N concentration, 4.5 atomic % (at. % or %). We synthesized the vertically aligned CNTs using the approximately same total flow rate (200 sccm) of CH_4 and NH_3 mixture. The N concentration of CNTs depends on the flow rate of NH_3 as shown in Table 1. The CNTs grown without the flow of NH_3 are doped with 2% N atoms. The N concentration can reach up to 6% for the CNTs grown at 1100 °C. It is noteworthy that the growth rate increases dramatically with the temperature, while it is insensitive to the flow rate of NH_3.

The N-doped CNTs were also synthesized by the thermal CVD of C_2H_2/NH_3 mixture at temperatures in the range of 900−1100 °C. The N content was adjustable by the flow rate of NH_3, as shown in Table 1. The CNTs are doped with 2% N atoms under no NH_3 flow. The concentration of N atoms increases to 5% when the flow rate of NH_3 is 40 sccm. The growth rate is independent of the N content in the range 2−5%. The growth rate is 7 ± 2, 14 ± 2, and 29 ± 5 μm/min, respectively, for 900, 1000, and 1100 °C, showing the 40-times enhancement of growth rate with the temperature. The growth rate was reproducible within the experimental error.

(2) The Dependence of C/N Composition on the Flow Rate of NH_3. Figure 2a shows the XPS data for the N-doped CNTs grown at 1000 °C using the CH_4/NH_3 mixture with a total flow rate of about 200 sccm. The flow rate of NH_3 is selected as 0, 5, and 40 sccm. The C 1s, N 1s, and O 1s peaks appear at 284.5, 400.7, and 532.9 eV, respectively. A strong and sharp peak at 284.5 eV confirms that the major component is carbon. The O peak arises from the oxygen in air and/or adsorbed on the surface of the nanotubes. The N content is 2.0, 3.3, and 4.7%, respectively, for 0, 5, and 40 sccm of the NH_3 flow rate.

Figure 2b shows a plot of the N content as a function of the NH_3 flow rate. Each data point is obtained using the flow rate of NH_3 as 0, 5, 20, 40, 50, 100, and 150 sccm. Total flow rate is about 200 sccm. As the flow rate of NH_3 increases, the N content increases from 2.0 to 4.7% then it decreases to 2.6%. The data are summarized in Table 1.We also changed the flow rate of CH_4 from 10 to 300 sccm and found that the nearly same N content was achieved for a given flow rate of NH_3. We obtained the maximum N content to be 4.4 and 6.0% for 900 and 1100 °C when the NH_3 flow rate is 30 and 100 sccm, respectively.

(3) Structure of the N-Doped CNTs. Figure 3 shows TEM images for the nanotubes grown at three temperatures, 900, 1000, and 1100 °C. As the temperature increases, the average diameter of CNTs increases from 40 to 150 nm and the diameter distribution becomes broader. The diameters of CNTs are

TABLE 1: Condition of NH_3 Pretreatment, Growth Rate, Diameter, Concentration of N Atoms, and Degree of Crystallinity of N-Doped CNTs Grown Using Thermal CVD of CH_4/NH_3 and C_2H_2/NH_3 Mixtures at Temperatures Ranging from 900 to 1000 °C

		NH_3 pretreatment								
	temp (°C)	flow rate (sccm)	time (min)	CH_4 or C_2H_2 flow rate (sccm)	NH_3 flow rate (sccm)	growth rate (μm/min)	diameter range (nm)	average diameter (nm)	at. % of N[a]	I_D/I_G[b]
$CH_4 + NH_3$	900	20	10	180	20	1 ± 1	30−70	50	4.4 ± 0.4	0.75 ± 0.08
	1000	20	5	200	0	2 ± 2	50−150	100	2.0 ± 0.2	0.48 ± 0.05
				200	5	3 ± 2			3.3 ± 0.3	0.61 ± 0.06
				180	20	3 ± 2			4.5 ± 0.4	0.66 ± 0.06
				160	40	3 ± 2			4.7 ± 0.4	0.66 ± 0.06
				150	50	3 ± 2			4.5 ± 0.4	−
				100	100	−[c]			3.2 ± 0.3	−
				50	150	−[c]			2.6 ± 0.2	0.43 ± 0.05
	1100	20	1	200	0	30 ± 5	100−200	150	2.0 ± 0.5	0.44 ± 0.04
				150	50	30 ± 5			4.5 ± 0.5	0.54 ± 0.05
				100	100	−[c]			6.0 ± 1.0	0.62 ± 0.06
$C_2H_2 + NH_3$	900	20	10	10	0	7 ± 1[d]	30−100	40	2 ± 0.5	0.65 ± 0.06
					40	7 ± 1			5 ± 0.5	0.86 ± 0.05
	1000	20	5	10	0	14 ± 3[d]	70−120	100	2 ± 0.5	0.67 ± 0.07
					40	14 ± 3		80	5 ± 0.5	0.82 ± 0.08
					80	14 ± 3		80	3.5 ± 0.5	0.70 ± 0.07
	1100	20	1	10	0	28 ± 5[d]	100−200	150	2 ± 0.5	0.45 ± 0.05
					20	28 ± 5			3 ± 0.5	0.60 ± 0.08

[a] Atomic % measured by XPS. [b] Intensity ratio of D band to G band in Raman spectrum. [c] Not vertically aligned. [d] Reference 36.

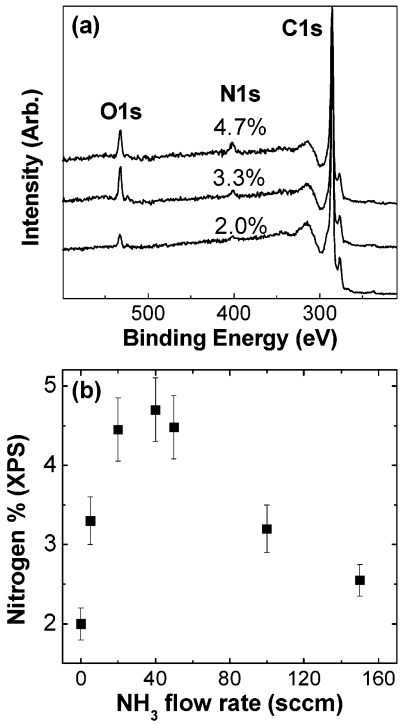

Figure 2. (a) XPS spectra of the N-doped CNTs grown at 1000 °C, showing 2.0, 3.3, and 4.7% N atoms. (b) A plot of the N content for the CNTs grown using various flow rates of NH_3 (sccm).

summarized in Table 1. For all temperatures, the nanotubes exhibit exclusively a bamboo-like structure in which the tube inside is separated into a series of compartments. The 2 and 5% N-doped nanotubes grown using C_2H_2/NH_3 mixture at 900 °C are shown in Figure 3, parts a and b, respectively. The 2.0 and 4.7% N-doped nanotubes grown using a CH_4/NH_3 mixture at 1000 °C are shown in Figure 3, parts c and d, respectively. Figure 3e and 3f correspond to the 2.0 and 4.5% N-doped nanotubes grown using CH_4/NH_3 mixture at 1100 °C, respectively. The structures of CNTs grown using C_2H_2 and CH_4 are similar for a given N % and temperature.

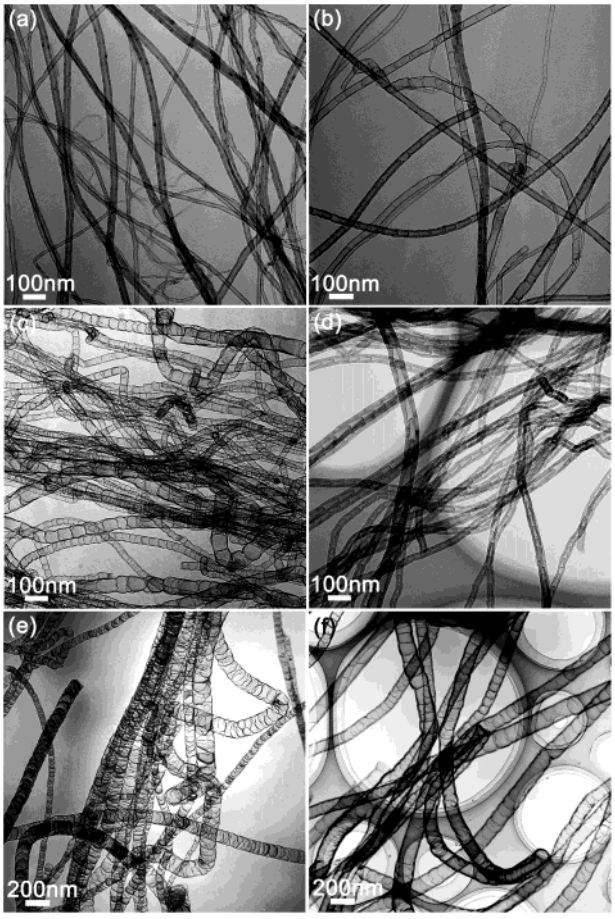

Figure 3. TEM images for (a) 2% and (b) 5% N-doped CNTs grown at 900 °C; (c) 2.0% and (d) 4.7% N-doped CNTs grown at 1000 °C; (e) 2.0% and (f) 4.5% N-doped CNTs grown at 1100 °C.

For 2% N-doped CNTs, the graphitic sheets separating the tube inside (so-called "compartment layers") are formed more randomly and frequently as the temperature increases (Figures 3a, 3c, and 3e). A close examination of the CNTs grown at

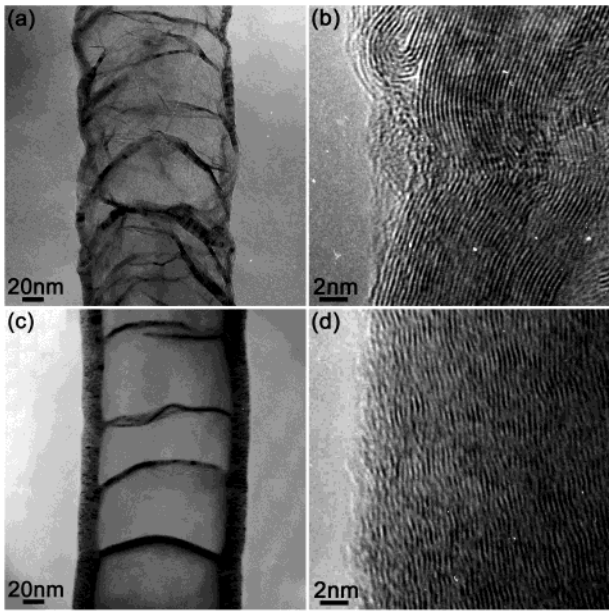

Figure 4. (a) HRTEM image for a 2.0% N-doped CNT grown at 1100 °C and (b) its atomic-resolved image. (c) HRTEM image for a 6.0% N-doped CNT grown at 1100 °C and (d) its atomic-resolved image. As the N content increases, the degree of crystalline perfection decreases.

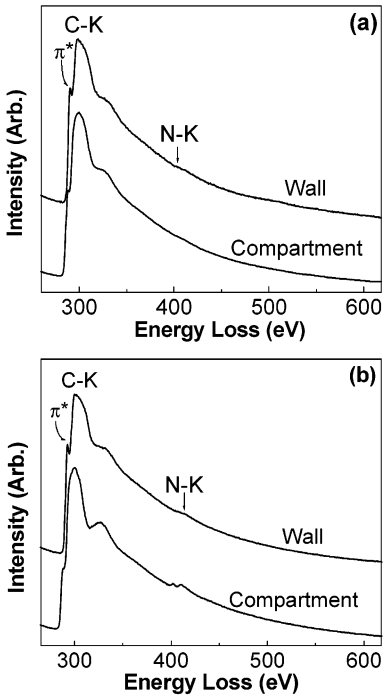

Figure 5. EELS data for the N-doped CNTs grown at 1100 °C, showing the K-shell ionization edges for carbon (C−K) and nitrogen (N−K). (a) The compartment layers and the wall contain 2% N atoms. (b) The compartment layers and the wall contain 9 and 4% N atoms, respectively.

900 °C reveals that the extremely thin compartment layers exist. At 1100 °C, a number of nanotubes show a nearly closed inside with the stacked compartment layers. The most distinctive structural change due to the increase of the N content is the appearance of the thick and curved compartment layers at a regular distance. As the concentration of N atoms in the CNTs grown at 900 °C increases from 2 to 4.7%, the compartment layers become more obvious (Figure 3, parts a and b). At 1000 °C, the higher concentration of N atoms induces the thicker compartment layers (Figure 3, parts c and d). At 1100 °C the highly N-doped CNTs look like springs due to the well-curved compartment layers at uniform distance (Figure 3f). As the N concentration increases, the number of compartment layers decreases while their thickness increases. The average number per micrometer is ∼20 and ∼10 for 2.0- and 4.5%-doped CNTs grown at 1100 °C, respectively.

Figure 4a corresponds to the high-resolution TEM (HRTEM) images for a 2.0% N-doped CNT grown at 1100 °C. The curvature of the compartment layers is oriented to the tip (top of the figure). The outer surface of the wall is not straight due to the randomly stacked compartment layers. The atomic-resolved image of the wall reveals the well-separated graphitic sheets by a distance of 0.34 nm (Figure 4b). As the N content increases to 6.0%, the compartment layers are smoothly curved to connect with the wall without distortion (Figure 4c). Thus the wall becomes straight and thicker. The graphitic sheets are waved over a long range, showing the lower degree of crystalline perfection than that of 2.0% N-doped CNTs (Figure 4d).

(4) The N Distribution in the N-Doped CNTs. The EELS data have been measured for the N-doped CNTs grown at 1100 °C whose N contents are determined as 2% (Figure 5a) and 6% (Figure 5b) using XPS. The EELS spectra are taken from two regions; the edge part of the wall and the compartment part. The spot size of the electron probe is about 2 nm. It shows two distinct absorption features starting at 284 and 400 eV, corresponding to the known K-shell ionization edges for carbon (C−K) and nitrogen (N−K), respectively. For C−K edge, a defining π^* peak at 300 eV corresponds to the graphitic carbons. Figure 5a shows that the N content is about 2% for both compartment and wall parts. The π^* peak of the C−K edge is stronger and sharper in the wall, compared to that of the compartment layers. It indicates that the crystallinity of the wall is higher than that of the compartment layers, even though the concentration of N atoms is the same.

In Figure 5b, the N content in the compartment layers is estimated as 9% while that in the wall is 4%. The average value is 6%, which is consistent with the XPS data. The π^* peak of C−K edge is stronger in the wall compared to the compartment layers. Therefore the compartment layers consist of the less crystalline graphitic sheets with the higher concentration of the N atoms than the wall.

(5) The Influence of the N Doping on the Crystallinity of Graphitic Sheets. Raman spectra taken from the 2.0, 3.3, and 4.7% N-doped CNTs grown using a CH_4/NH_3 mixture at 1000 °C are displayed in Figure 6a. Each spectrum is the average of many samples. All spectra show mainly two bands at ∼1350 cm^{-1} (D band) and ∼1576 cm^{-1} (G band). The G band originates from the Raman active E_{2g} mode due to in-plane atomic displacements. The origin of D band has been explained as disorder-induced features due to the finite particle size effect or lattice distortion.[33−35] As the concentration of the N atoms increases, the D band becomes stronger and broader. The linear relation between the inverse of the in-plane crystallite dimension and the intensity ratio of D band to G band (I_D/I_G) was noted.[35] The value of I_D/I_G increases from 0.48 to 0.66 as the N content increases from 2.0% to 4.7%. The value of I_D/I_G for the N-doped CNTs grown at three temperatures is plotted in Figure 6b. The data show that the degree of long-range ordered crystalline perfection increases with the temperature, but decreases by the N doping. The data of the N-doped CNTs grown using C_2H_2/NH_3 mixture are listed in Table 1. The value of I_D/I_G usually decreases by about 0.2 for the increase of the N content from 2 to 5%.

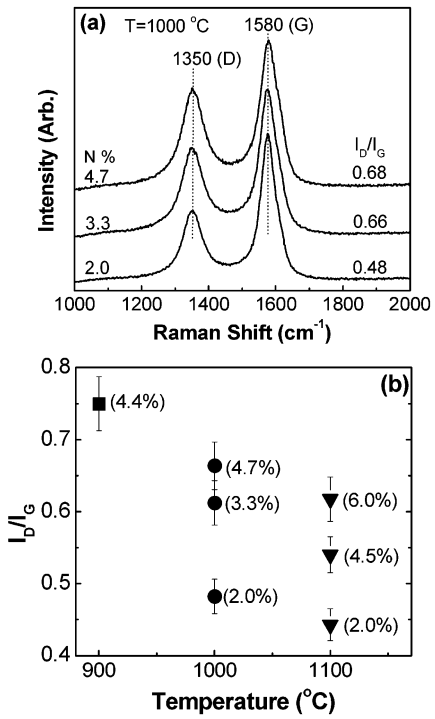

Figure 6. (a) Raman spectrum for 2.0, 3.3, and 4.7% N-doped CNTs grown at 1000 °C. (b) Plot of the I_D/I_G value vs the N content and growth temperature. The data in parentheses represent the N content obtained from the XPS analysis.

4. Discussion

We previously reported the vertically aligned CNTs using the thermal CVD of C_2H_2 in the temperature range 800−1100 °C.[36] Even if no NH_3 flows during the growth, those CNTs were doped with 2% N atoms as shown in Table 1. Under our experimental condition, the growth of CNTs is possible only when NH_3 is used as a pretreatment gas. The role of NH_3 is the formation of Fe catalytic nanoparticles via etching. Ar flushes at least 10 min before the flow of C_2H_2, to eliminate the residual NH_3 in the reactor. However, the N doping still occurs with the same concentration, 2%. Therefore we suggest that the NH_3 etching would inevitably dissolve the N atoms into the Fe nanoparticles. These dissolved N atoms would precipitate with the C atoms during the growth of CNTs, following the base growth mechanism. We'll discuss a detailed growth mechanism in the following paragraph. We were able to increase the N content of CNTs simply by flowing NH_3 with C_2H_2 (or CH_4) during the growth. But it is not clear to explain why the N content decreases at the higher flow rate of NH_3. The maximum N content in the present CNTs is about 6%, which is consistent with the result of other groups that the N content usually did not exceed 10%.

The growth rate of N-doped CNTs is nearly the same for the N content ranging from 2 to 5%. For the vertically aligned CNTs (doped with 2% N atoms) grown using C_2H_2, the growth rate as a function of temperature has been discussed in ref 36. The Arrhenius plot of the growth rate yields an activation energy that is almost the same as the diffusion energy of C atom in the γ-phase Fe. Moreover, the growth of nanotubes has been suitably explained by the assumption that the rate-determining step is a diffusion-controlled first-order reaction.[37] It implies that the growth rate of nanotubes would be proportional to the diffusion coefficient of C atom and the saturated C concentration in the bulk. The diffusion of N atoms probably involves in the growth of nanotubes. However, for the doping of 2−6% N atoms, its contribution would be negligible compared to that of C atom. The growth rate of CNTs can be thus determined mainly by the bulk diffusion rate of C atoms.

The use of CH_4 as the C source has been rarely reported for the growth of the vertically aligned CNTs using thermal CVD. It is related with the fact that the thermal decomposition of CH_4 is not as efficient as that of other C sources such as C_2H_2 or ethylene (C_2H_4). To our best knowledge, it is first time to report the vertically aligned CNTs using thermal CVD of CH_4 at temperatures down to 900 °C. The growth rate of N-doped CNTs at 1100 °C is essentially the same for both CH_4/NH_3 and C_2H_2/NH_3 mixtures. However, the growth rate of CNTs using CH_4/NH_3 mixture is lower than that using C_2H_2/NH_3 mixture. To understand the effect of the C source on the growth rate, we synthesized the vertically aligned CNTs on the Fe-deposited Si substrates using C_2H_4 and ethane (C_2H_6) in the temperature range 800−1100 °C. It shows the same growth rates as those of CNTs grown using C_2H_2. The growth rate depending on the C source will be rigorously discussed in a separated paper. Here, we suggest that the decomposition of C_2H_2, C_2H_4, and C_2H_6 at temperatures in the range 800−1100 °C would generate the saturated C concentration in gas phase, leading the same growth rate of CNTs. However, CH_4 may provide the saturated concentration only when the temperature is as high as 1100 °C.

In contrast to the insensitive growth rate on the N content, the overall structure of N-doped CNTs depends on not only the temperature but also the N content. The average diameter and the diameter range usually increase with the temperature, due to the more efficient agglomeration of the Fe catalytic nanoparticles. The bamboo-like structure of the 2% N-doped CNTs has been described thoroughly using the base growth mechanism.[36−38] The growth process was separated into five steps: (i) the formation of the closed tip, (ii) the growth of the wall, (iii) the production of the compartment layers, (iv) the formation of the joint between compartment layers and wall, and (v) the production of the bamboo-like structure owing to the periodic compartment layers. In each step, the bulk diffusion of C atom in the catalytic particles plays an important role.

As the temperature increases, the surface and bulk diffusion rates of C atoms can increase. If the bulk diffusion rate increases more significantly compared to that of surface diffusion, the growth rate of compartment layers would be greatly enhanced. The compartment layers are therefore formed with a larger thickness, connected with the wall more frequently.[36] As the growth rate of the compartment layers overwhelms that of the wall, the compartment layers are eventually nested to construct the tube. When the compartment layers depart from the catalytic particle, the motive force could be the stress accumulated under the graphitic cap formed on the catalytic nanoparticles. If the degree of the crystalline perfection were high, the thick compartment layers would be curved under a larger strain and seriously distort the wall structure.

As the N atoms incorporate into the graphitic sheets, the crystalline perfection of the graphitic sheets deteriorates. This result is consistent with the work of other groups.[19−32] The pyridine-typed N atoms would reduce the crystalline perfection of the graphitic sheets.[19] The less crystalline graphitic sheets probably exhibit more flexibility. Then the compartment layers are smoothly bent and the connection with the wall would take place under less strain. After the joint, the graphitic sheets of compartment layers and wall would grow at the same rate and eventually depart from the catalytic particle. If the stress were release, this joint growth would take longer before departing from the catalytic particle, resulting in the increase of the wall

thickness and less frequent formation of the thicker compartment layers.

The compartment layers of the highly doped CNTs exhibit more N content than the wall. Han et al. also reported the higher N concentration of the compartment layers compared to the wall.[20] The EELS data reveal that the degree of crystalline perfection is always lower for the compartment layers compared to that of the wall, even if the N concentration is the same for both parts. It must be related to the fact that the graphitic sheets of the compartment layers intrinsically contain more defects due to the curved feature. In the case of the CNTs doped with the higher N atoms, the N doping occurs preferentially in the defect sites at the curved graphitic sheets of compartment layers. The N-doped graphitic sheets of the compartment layers are thus released from the strain when connecting with the wall. The shape of compartment layers can be notably changed due to the more significant doping of N atoms. We conclude that the doping of N atoms plays a significant role in modifying the structure of bamboo-like CNTs.

5. Conclusion

The vertically well-aligned N-doped CNTs were grown on the Fe nanoparticles deposited Si substrates using thermal CVD of CH_4/NH_3 and C_2H_2/NH_3 mixtures in the temperature range 900−1100 °C. The N content in the range 2−6% has been controlled by the flow rate of NH_3. The growth rate is almost independent of the N content. However, the N doping modifies remarkably the structure and the degree of crystallinity of CNTs. The bamboo-like structured CNTs are exclusively produced. As the N content increases, the more curved and thicker compartment layers appear more regularly at the longer distance. The HRTEM images and Raman spectra reveal consistently that as the N content increases the degree of crystalline perfection decreases. The EELS data indicate the higher N % in the less crystalline compartment layers compared to the wall.

The dependence of the growth rate, the structure, and the crystallinity on the N content has been explained by adopting the base growth mechanism of CNTs. We suggest that the growth rate would be mainly determined by the bulk diffusion rate of C atoms. The N doping would enhance the flexibility of the graphitic sheets. Then the compartment layers are bent and connect with the wall under less strain. The joint growth of the wall and compartment layers would also take longer due to the reduced strain. The present result shows that the N doping is one of promising ways to control the crystallinity and structure of nanotubes.

Acknowledgment. This work was supported by Direct Basic Research Program (Korea Science and Engineering foundation Project No. R04-2002-000-20088-012003). SEM analyses were partly performed at the Korea Basic Science Institute in Seoul.

References and Notes

(1) de Heer, W. A.; Châtelain, A.; Ugarte, D. *Science* **1995**, *270*, 1179.
(2) Rinzler, A. G.; Hafner, J. H.; Nikolaev, P.; Lou, L.; Kim, S. G.; Tomanek, D.; Nordlander, P.; Colbert, D. T.; Smalley, R. E. *Science* **1995**, *269*, 1550.
(3) Rosen, R.; Simendinger, W.; Debbault, C.; Shimoda, H.; Fleming, L.; Stoner, B.; Zhou, O. *Appl. Phys. Lett.* **2000**, *76*, 1668.
(4) Biercuk, M. J.; Llaguno, M. C.; Radosavljevic, M.; Hyun, J. K.; Johnson, A. T.; Fischer, J. E. *Appl. Phys. Lett.* **2002**, *80*, 2767.
(5) Glatkowski, P.; Mack, P.; Conroy, J. L.; Piche, J. W.; Winsor, P. U.S. Patent 6,265,466, 2001.
(6) Liang, W.; Bockrath, M.; Bozovic, D.; Hafner, J. H.; Tinkham, M.; Park, H. *Nature* **2001**, *411*, 665.
(7) Tans, S. J.; Verschueren, A. R. M.; Dekker, C. *Nature* **1998**, *393*, 49.
(8) Bachtold, A.; Hadley, P.; Nakanishi, T.; Dekker, C. *Science* **2001**, *294*, 1317.
(9) An, K. H.; Kim. W. S.; Park, Y. S.; Moon, J.-M.; Bae, D. J.; Lim, S. C.; Lee, Y. S.; Lee, Y. H. *Adv. Funct. Mater.* **2001**, *11*, 387.
(10) Liu, C.; Fan, Y. Y.; Liu, M.; Cong, H. T.; Cheng, H. M.; Dresselhaus, M. S. *Science* **1999**, *286*, 1127.
(11) Bethune, D. S.; Kiang, C. H.; deVries, M. S.; Gorman, G.; Savoy, R.; Vazquez, J.; Beyers, R. *Nature* **1993**, *363*, 605.
(12) Journet, C.; Maser, W. K.; Bernier, P.; Loiseau, A.; Lamy de la Chapelle, M.; Lefrant, S.; Deniard, P.; Lee, R.; Fischer, J. E. *Nature* **1997**, *388*, 756.
(13) Thess, A.; Lee, R.; Nikolaev, P.; Dai, H.; Petit, P.; Robert, J.; Xu, C.; Lee, Y. H.; Kim, S. G.; Rinzler, A. G.; Colbert, D. T.; Scuseria, G. E.; Tomanek, D.; Fisher, J. E.; Smalley, R. E. *Science* **1996**, *273*, 483.
(14) Terrones, M.; Grobert, N.; Olivares, J.; Zhang, J. P.; Terrones, H.; Kordatos, K.; Hsu, W. K.; Hare, J. P.; Townsend, P. D.; Prassides, K.; Cheetham, A. K.; Kroto, H. W.; Walton, D. R. M. *Nature* **1997**, *388*, 52.
(15) Ren, Z. F.; Huang, Z. P.; Xu, J. W.; Wang, J. H.; Bush, P.; Siegal, M. P.; Provencio, P. N. *Science* **1998**, *282*, 1105.
(16) Fan, S.; Chapline, M. G.; Franklin, N. R.; Tombler, T. W.; Cassell, A. M.; Dai, H. *Science* **1999**, *283*, 512.
(17) Terrones, M.; Ajayan, P. M.; Banhart, F.; Blase, X.; Carroll, D. L.; Charlier, J. C.; Crzerw, R.; Foley, B.; Grobert, N.; Kamalakaran, R.; Kohler-Redlich, P.; Rühle, M.; Seeger, T.; Terrones, H. *Appl. Phys. A* **2002**, *74*, 355.
(18) Terrones, M.; Redlich, P.; Grobert, N.; Trasobares, S.; Hsu, W. K.; Terrones, H.; Zhu, Y. Q.; Hare, J. P.; Reeves, C. L.; Cheetham, A. K.; Rühle, M.; Kroto, H. W.; Walton, D. R. M. *Adv. Mater.* **1999**, *11*, 655.
(19) Terrones, M.; Terrones, H.; Grobert, N.; Hsu, W. K.; Zhu, Y. Q.; Hare, J. P.; Kroto, H. W.; Walton, D. R. M.; Redlich, P.; Rühle, M.; Zhang, J. P.; Cheetham, A. K. *Appl. Phys. Lett.***1999**, *75*, 3932.
(20) Han, W. Q.; Redlich, P.; Seeger, T.; Ernst, F.; Rühle, M.; Grobert, N.; Hsu, W. K.; Chang, B. H.; Zhu, Y. Q.; Kroto, H. W.; Walton, D. R. M.; Terrones, M.; Terrones, H. *Appl. Phys. Lett.* **2000**, *77*, 1807.
(21) Ma, X.; Wang, E.; Zhou, W.; Jefferson, D. A.; Chen, J.; Deng, S.; Xu, N.; Yuan. J. *Appl. Phys. Lett.* **1999**, *75*, 3105.
(22) Zhong, D.; Liu, S.; Zhang, G.; Wang, E. G. *J. Appl. Phys.* **2001**, *89*, 5939.
(23) Ma, X.; Wang, E. G. *Appl. Phys. Lett.* **2001**, *78*, 978.
(24) Wang, E. G. *J. Am. Ceram. Soc.* **2002**, *85*, 105.
(25) Nath, M.; Satishkumar, B. C.; Govindaraj, A.; Vinod, C. P.; Rao, C. N. R. *Chem. Phys. Lett.* **2000**, *322*, 333.
(26) Sen, R.; Satishkumar, B. C.; Govindaraj, A.; Harikumar, K. R.; Raina, G.; Zhang, J. P.; Cheetham, A. K.; Rao, C. N. R. *Chem. Phys. Lett.* **1998**, *287*, 671.
(27) Yudasaka, M.; Kikuchi, R.; Ohki, Y.; Yoshimura, S. *Carbon* **1997**, *35*, 195.
(28) Suenaga, K.; Yudasaka, M.; Colliex, C.; Iijima, S. *Chem. Phys. Lett.* **2000**, *316*, 365.
(29) Sung, S. L.; Tsai, S. H.; Tseng, C. H.; Chiang, F. K.; Liu, X. W.; Shin, H. C. *Appl. Phys. Lett.* **1999**, *74*, 197.
(30) Kurt, R.; Klinke, C.; Bonard, J. M.; Kern, K.; Karimi, A. *Carbon* **2001**, *39*, 2163.
(31) Lee, C. J.; Lyu, S. C.; Kim, H. W.; Lee, J. H.; Cho, K. I. *Chem. Phys. Lett.* **2002**, *359*, 115.
(32) Wang, X.; Liu, Y.; Zhu, D.; Zhang, L.; Ma, H.; Yao, N.; Zhang, B. *J. Phys. Chem. B* **2002**, *106*, 2186.
(33) Tuinstra, F.; Koenig, J. L. *J. Chem. Phys*. **1970**, *53*, 1126.
(34) McCulloch, D. G.; Prawer, S.; Hoffman, A. *Phys. Rev. B* **1994**, *50*, 5905.
(35) Wilhelm, H.; Lelaurain, M.; McRae, E.; Humbert, B. *J. Appl. Phys.* **1998**, *84*, 6552.
(36) Lee, Y. T.; Park, J.; Choi, Y. S.; Ryu, H.; Lee, H. J. *J. Phys. Chem. B* **2002**, *106*, 7614.
(37) Kim, N. S.; Lee, Y. T.; Park, J.; Ryu, H.; Lee, H. J.; Choi, S. Y.; Choo, J. *J. Phys. Chem.* B **2002**, *106*, 9286.
(38) Lee, C. J.; Park, J. *J. Phys. Chem. B* **2001**, *105*, 2365.